ACS NANO

www.acsnano.org

ARTICLE

Extinction-to-Absorption Ratio for Sensitive Determination of the Size and Dielectric Function of Gold Nanoparticles

Aleksa Djorović, Steven J. Oldenburg, Johan Grand, and Eric C. Le Ru*

Cite This: *ACS Nano* 2020, 14, 17597−17605

Read Online

ACCESS | Metrics & More | Article Recommendations | Supporting Information

ABSTRACT: **Gold nanoparticles (AuNPs) have become an essential tool for a variety of fields across the biological, physical, and chemical sciences. The characterization of AuNPs by UV−vis spectroscopy is simple and commonly used but remains prone to error because of size and shape polydispersity and uncertainties in the dielectric function. We here propose and demonstrate a method to significantly improve this routine characterization technique by measuring not only the extinction but also the absorption spectrum. Specifically, we show that by considering the ratio of the extinction to absorption spectra, denoted η, we are able to determine the volume of AuNPs with a significant increase in accuracy compared to the UV−vis extinction method. We also prove an important property of η: it is independent of particle shape within the quasi-static/dipolar approximation, typically for particle sizes up to 100 nm. This shape independence results in very strong constraints for the theoretical predictions to agree with the experiments. We show that the spectral shape of η can therefore be used to discriminate between different proposed data sets for the dielectric function of gold, a long-standing challenge in plasmonics research.**

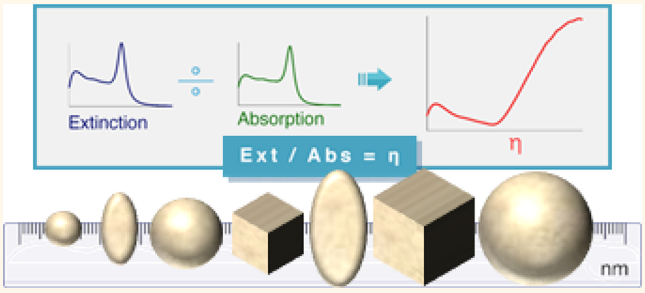

KEYWORDS: *nanoparticles, size determination, dielectric function, extinction spectroscopy, absorption spectroscopy, plasmonics*

Gold nanoparticles (AuNPs) are an essential and ubiquitous tool in nanotechnology, owing largely to their localized surface plasmon (LSP) resonance[1,2] but also to their biocompatibility,[3,4] chemical stability, and ease of conjugation and functionalization.[5] As such, they have found diverse applications as biomarkers[6] and building blocks in nanotechnology but also in medical detection and diagnostics,[7] therapeutics,[8] drug delivery,[9] catalysis,[10] Raman and fluorescence spectroscopy,[11] and optical sensing.[8,12] These applications often rely on a well-defined size, shape, and concentration of the AuNPs, which themselves determine the optical, electrical, chemical, and biological properties.[13,14] As a result, the characterization of these properties is critical and has been the focus of much effort.

Various tools have been developed for delicate size and shape control of AuNPs as well as for their characterization. While transmission electron microscope (TEM) imaging[15,16] is the *defacto* well-established primary method, there have been efforts to measure NP size through methods that are faster, more easily accessible, and less expensive. Among those, dynamic light scattering[17−19] and nanoparticle tracking analysis[20,21] are routinely used, but they measure the hydrodynamic diameter, which is nontrivially related to the shape and also depends on surface adsorbates. These techniques, as well as TEM, are also not well suited to concentration estimates. The other common characterization tool is UV−vis extinction spectroscopy,[8,14] which can be used in conjunction with electromagnetic theoretical simulations to determine both NP size and concentration, providing the shape is defined. This approach largely alleviates the need for TEM imaging once the shape-controlled synthesis has been optimized. It is however not as precise as TEM for size measurement, by a long way. The agreement between experimental extinction spectra and theory also tends to show some discrepancies in the peak position or overall spectral shape, which are commonly attributed to effects such as a distribution of particle size and shape,[22] aggregation, or uncertainty on the gold dielectric function. With careful

Received: October 8, 2020
Accepted: December 7, 2020
Published: December 11, 2020

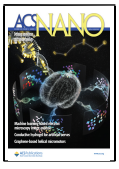

https://dx.doi.org/10.1021/acsnano.0c08431
ACS Nano 2020, 14, 17597−17605

accounts of these effects, some success has been demonstrated in quantitatively predicting particle size and concentration in the special case of nanospheres[8,14] and nanorods.[22] Nevertheless, the extinction spectrum alone remains too insensitive to size to provide a high level of accuracy, reliability, and convenience in the size determination, especially for nonspherical particles.

To overcome this issue, we recently proposed to complement the extinction spectrum with an additional absorption spectrum measurement.[23] Such a measurement is in practice possible by measuring the optical transmission of the sample embedded in an integrating sphere.[23−29] In ref 23, it was in particular shown that the combined absorption/extinction spectra analysis provided insight into shape imperfections of silver NPs. In this work, we focus more specifically on gold NPs and on the extinction-to-absorption ratio spectrum $\eta(\lambda)$, which is a concentration-independent quantity that can be readily derived from the combined extinction/absorption measurement. We show experimentally, and explain theoretically, that the wavelength-dependent extinction-to-absorption ratio $\eta(\lambda)$ is extremely sensitive to NP volume and can be used to determine the volume of AuNPs and, therefore, its dimensions if the shape is defined, which is significantly better than using solely extinction. It can clearly differentiate between 50 and 60 nm gold nanospheres even in the presence of size and shape distribution. Interestingly, we show that $\eta(\lambda)$ is in fact independent of shape in the small size regime (approximately up to a volume equivalent radius of ∼100 nm) and therefore provides a general method for determining NP volume in this range. Finally, the large sensitivity to volume of the ratio η, together with the shape independence, results in very strong constraints for theoretical predictions to agree with the experiments, which can be exploited to test several gold dielectric function models against the experiments. This provides direct insight into this crucial parameter, which cannot be easily inferred from any other techniques. Using spherical NPs with high uniformity in size and shape, we are able to show that only some models of the gold dielectric function are compatible with the measured spectral shape of η. This provides an experimentally-based approach to choose the correct gold dielectric function to use in theoretical calculations of AuNPs, which has been a long-standing challenge in plasmonics research.

RESULTS AND DISCUSSION

Extinction-to-Absorption Ratio as a Metric for Gold Nanosphere Size. UV−vis extinction spectroscopy has long been used to infer gold nanosphere size. However, extinction spectra commonly do not show an exact agreement with electromagnetic theory predictions (see Figure 1a). This discrepancy is often ignored and attributed to particle imperfections and size distribution.[8,14] Another particular issue when comparing experimental extinction data to theoretical predictions is the choice of NP material dielectric function. This issue has recently become even more evident with several literature reports of newly measured sets of data for the dielectric function of gold,[30,32,33] which differ from each other and from the commonly used Johnson and Christy data.[31,34] The different choices of dieletric function can lead to different plasmon resonance position and therefore different size predictions, as exemplified in Figure 1e. This is compounded by the fact that the overall extinction spectrum is not strongly sensitive to size. As shown in Figure 1e, the

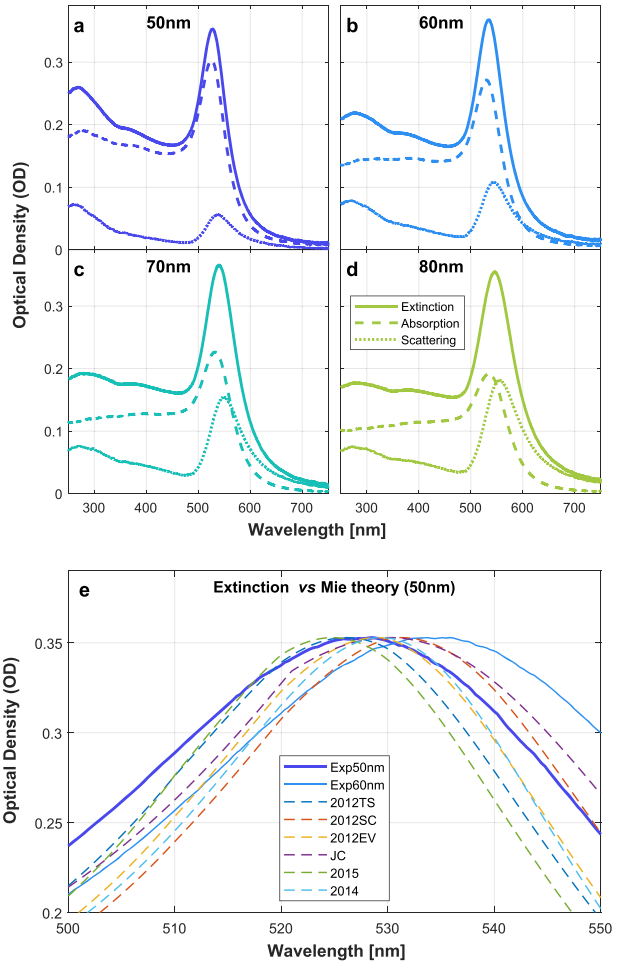

Figure 1. Measured extinction, absorption, and scattering spectra of gold NPs of (a) 50, (b) 60, (c) 70, and (d) 80 nm diameter. The measured extinction spectra are compared in (e) to the theoretical predictions from the Mie theory for a 50 nm gold sphere using a selection of dielectric functions of gold reported in the literature: Template-stripped (2012TS), single crystal (2012SC), and evaporated (2012EV) gold from ref 30, Johnson and Christy (JC),[31] and two other recent measurements from ref 32 (2015) and ref 33 (2014).

resonance shifts by only 7 nm between the diameters of 50 and 60 nm, which is about the same shift as observed for 50 nm NPs modeled with two different dielectric functions. The extinction spectrum cannot therefore provide an accurate method to infer size and, therefore, concentration. We will come back at the end to the issue of choice of the dielectric function, and for now, we will use the dielectric function for single crystal gold (2012SC) from ref 30 for all further calculations, as it does not affect our conclusions.

We here aim to overcome this problem by exploiting the additional information obtained from concurrently measuring absorption spectra. This can be achieved with an integrating sphere setup,[23,25,28,29] as described in the Methods section. Experimental extinction and absorption and, therefore, scattering spectra were measured for spherical citrate-reduced AuNPs with nominally 50, 60, 70, and 80 nm diameter and are summarized in Figure 1a−d. It is interesting to note that the absorption resonances are slightly blue-shifted from those of the scattering, as predicted by the Mie theory, but the size dependence of the resonance position is not more pronounced

https://dx.doi.org/10.1021/acsnano.0c08431
ACS Nano 2020, 14, 17597−17605

than for extinction. What is clear from Figure 1a–d, however, is that the relative intensity of the extinction and absorption spectra changes significantly over this size range.

This suggests that we should consider the extinction-to-absorption ratio spectra $\eta(\lambda)$, which are shown in Figure 2.

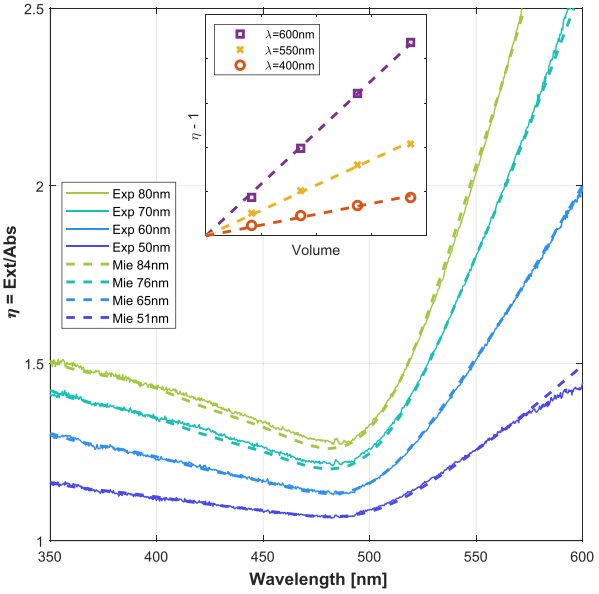

Figure 2. Experimentally derived extinction-to-absorption ratio η for nominally 50, 60, 70, and 80 nm AuNPs. These are compared to Mie theory predictions for the best fitting size in each case: 51, 65, 76, and 84 nm. Note that, beyond 600 nm, both absorption and extinction are small (under 0.01 OD), and their ratio therefore has large uncertainties and cannot be obtained reliably. The inset shows $\eta - 1$ at selected wavelengths as a function of NP volume V (using the Mie-derived diameter).The straight lines are linear fits through the origin.

One first advantage of this ratio is that it is intrinsically independent of concentration. Moreover, in contrast to extinction, the $\eta(\lambda)$ spectra clearly differentiate particle size across almost the entire spectrum and particularly in the region above the main plasmon resonance (530–600 nm). The extinction-to-absorption ratio spectrum, $\eta(\lambda)$, therefore provides a much more sensitive size determination method for spherical AuNPs in this size range compared to using solely extinction spectra. Note also that the $\eta(\lambda)$ spectrum, contrarily to extinction and absorption, does not exhibit any feature associated with the LSP resonance. The experimental data are compared in Figure 2 to Mie Theory predictions, where the only free parameter, the NP diameter, was adjusted to obtain the best fit to the experimental data. We observe excellent agreement between the model and experiment in the spectral shape across the entire window of interest. We will explain the reasons for the small remaining discrepancy between the nominal and fitted sizes in the following.

The strong dependence of η on size can be simply understood in the quasi-static/dipolar approximation to EM scattering.[11] First, let us note that η can be expressed as

$$\eta = \frac{\langle C_{ext}\rangle}{\langle C_{abs}\rangle} = 1 + \frac{\langle C_{sca}\rangle}{\langle C_{abs}\rangle} \quad (1)$$

where $\langle C_{ext}\rangle$, $\langle C_{abs}\rangle$, and $\langle C_{sca}\rangle = \langle C_{ext}\rangle - \langle C_{abs}\rangle$ denote the orientation-averaged extinction, absorption, and scattering cross sections. For very small particles with negligible scattering compared to absorption, we therefore expect $\eta \approx 1$. More quantitatively, the optical response of the NP can be modeled as that of an induced dipole with a polarizability α proportional to the NP volume V.[11,35,36] Absorption is then proportional to $\mathrm{Im}(\alpha)$, *i.e.*, to V, whereas scattering is proportional to $|\alpha|^2$, *i.e.*, V^2, and thus one, expects $\eta - 1$ to be proportional to the NP volume V. This linear dependence on volume is confirmed experimentally as shown in the inset of Figure 2. Because the volume is proportional to the cube of the NP size, this results in a very strong dependence of η on NP size.

From this dependence, we can also infer the expected size range where the method will work best. For spheres below 25 nm in diameter, η is less than 1.1 over the entire spectral range, so both absorption and extinction spectra would have to be measured with an accuracy of a few percent to get meaningful results in this range, which is beyond what we can achieve with the method we used. We note that this is also the size regime where surface scattering effects must be taken into account in the dielectric function to obtain quantitative predictions.[8] In the size range of 25–150 nm, η is very sensitive to size and varies approximately linearly with volume, especially for the smaller sizes. This is the optimal size range for the application of this method. For sizes above 150 nm, the relationship between η and size becomes more complicated and becomes dominated by retardation effects.

Effect of Size Distribution on the Extinction-to-Absorption Ratio. We now investigate the effect of a distribution of NP sizes on η using predictions from the Mie theory. We use nanospheres of 50 nm diameter for illustration, but the conclusions are general. Representative extinction, absorption, and extinction-to-absorption ratio spectra are shown in Figure 3a–c. The dispersion of NP diameters is taken as a Gaussian distribution centered on 50 nm with standard deviation σ of 3, 5, or 10 nm. The corresponding size distributions are plotted in Figure 3d–f. These are also compared to the predictions for perfectly monodisperse 50, 52, and 55 nm nanospheres. The first observation is that a typical distribution of particle sizes (like the ones considered here) will only result in small changes in extinction, absorption, and η. Nevertheless, we see in Figure 3c that the size dispersity does result in a small increase in predicted size when using the ratio η as the determination metric. This is understandable, as the larger particles contribute more than the smaller ones to the extinction and absorption spectra due to the V^2 and V dependence; η is therefore biased toward the large-size side of the distribution. This effect is small: even for a relatively large size distribution with σ = 10 nm (Figure 3f), the η spectrum resembles that of a 55 nm-diameter monodisperse sphere, *i.e.*, a 10% overestimate. More realistic distributions result in closer to a 5% overestimate; for example, 50 ± 5 nm is close to a 52 nm monodisperse sphere. We do observe a secondary effect of the size distribution: it introduces subtle changes in the wavelength dependence of η with the monodisperse case being slightly larger in the 500–500 nm range and below 400 nm. Despite this, we conclude that the η ratio is to a good approximation independent of the size distribution, but in cases where high-accuracy size determination is required, it should be accounted for explicitly using the Mie theory, or a 5% overestimate can be assumed for typical size distributions of gold nanosphere solutions. This explains the apparent discrepancy between nominal and fitted diameter in Figure 1.

https://dx.doi.org/10.1021/acsnano.0c08431
ACS Nano 2020, 14, 17597–17605

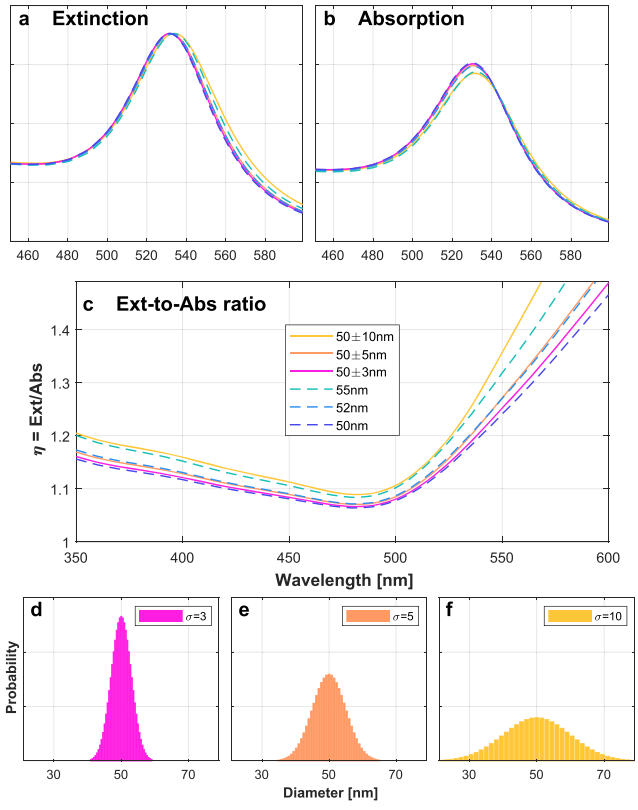

Figure 3. Predicted extinction (a), absorption (b), and extinction-to-absorption ratio η (c) for spherical AuNPs with mean Gaussian size distributions of 50 nm and standard deviation σ of 3, 5, and 10 nm. These distributions are shown in panels d–f. Also included for comparison in panels a–c are the predictions for perfectly monodisperse spheres of diameters 50, 52, and 55 nm.

More quantitative fits of these experimental data will be further discussed later.

Extension to Nonspherical Particles. As discussed for spheres, the dependence of η on volume V can be explained simply within the quasi-statics approximation. We now re-examine this argument for a general nonspherical particle. The dipolar approximation can also be applied, and the polarizability remains proportional to V, resulting in $\eta - 1 \sim V$, albeit, *a priori*, with a shape-dependent proportionality coefficient. In order to be more quantitative, we restrict ourselves to axi-symmetric particles (around z) for which simple analytic expressions exist for the polarizability tensor $\underline{\alpha}$.[35] Using SI units, we first define the normalized adimensional polarizability tensor $\underline{\beta}$ such that

$$\underline{\alpha} = \epsilon_0 \epsilon_M V \underline{\beta} \tag{2}$$

We then have (extending the results of ref 35 to a general embedding medium with dielectric constant ϵ_M):

$$\beta_{xx} = \beta_{yy} = \frac{\epsilon - \epsilon_M}{\epsilon_M + (\epsilon - \epsilon_M)\left(\frac{1}{3} - I\right)} \tag{3}$$

$$\beta_{zz} = \frac{\epsilon - \epsilon_M}{\epsilon_M + (\epsilon - \epsilon_M)\left(\frac{1}{3} + 2I\right)} \tag{4}$$

where $\epsilon(\lambda)$ is the dielectric function of gold and I is a shape-dependent real constant, which can be expressed as an integral on the particle surface[35] but whose value will be irrelevant here. The orientation-averaged cross sections within the quasi-static/dipolar approximation are then obtained from[11,36,37]

$$\langle C_{abs} \rangle = \frac{k_M}{3\epsilon_0 \epsilon_M} [\mathrm{Im}(\alpha_{zz}) + 2\mathrm{Im}(\alpha_{xx})] \tag{5}$$

$$\langle C_{sca} \rangle = \frac{(k_M)^4}{18\pi(\epsilon_0 \epsilon_M)^2} [|\alpha_{zz}|^2 + 2|\alpha_{xx}|^2] \tag{6}$$

where $k_M = (2\pi/\lambda)\sqrt{\epsilon_M}$ is the wavevector in the embedding medium. We then notice the important property (for $u = x, y, z$):

$$\mathrm{Im}\left(\frac{1}{\beta_{uu}}\right) = \mathrm{Im}\left(\frac{\epsilon_M}{\epsilon - \epsilon_M}\right) \tag{7}$$

which is independent of I and therefore of shape, from which we also deduce that

$$\mathrm{Im}(\beta_{uu}) = -\mathrm{Im}\left(\frac{\epsilon_M}{\epsilon - \epsilon_M}\right)|\beta_{uu}|^2 \tag{8}$$

Combining it all together, we deduce that η is also independent of shape and obtain an explicit expression:

$$\eta - 1 = \frac{\langle C_{sca} \rangle}{\langle C_{abs} \rangle} = -\frac{V}{6\pi} \frac{(k_M)^3}{\mathrm{Im}\left(\frac{\epsilon_M}{\epsilon - \epsilon_M}\right)} \tag{9}$$

Equation 9 is a universal property in the quasi-static/dipolar approximation, independent of shape. It fully specifies the volume and wavelength dependence of η in this approximation, which should be valid in the limit of small size. This has several implications. First, for all shapes, $\eta - 1$ is proportional to volume and therefore very sensitive to size. More importantly, $\eta - 1$ should be shape independent in the regime where the quasi-static approximation is valid. It therefore provides an absolute measurement of NP volume in this regime. Another corollary is that η is independent of the LSP resonance of the NP, which is therefore not visible (as a peak or trough) in the spectrum of $\eta(\lambda)$, as confirmed for nanospheres in Figure 2.

To illustrate these further, we carried out numerical computations of the orientation-averaged optical properties of particles of various shapes and sizes: spheres, prolate spheroids of aspect ratio $h = 2$ and $h = 5$, nanorods of aspect ratio 3, and nanocubes. We compare in particular particles of different shapes but the same volume V, identified by the equivalent radius r_{eq} or diameter d_{eq} of a sphere of the same volume. The results are summarized in Figure 4 where $\eta(\lambda)$ is compared to the quasi-statics approximation expression, eq 9. As seen in Figure 4a,b, the extinction and absorption spectra for $d_{eq} = 60$ nm are strongly shape dependent, as expected. Because of the orientation averaging, elongated NPs exhibit two dipolar LSP resonances associated with transverse and longitudinal excitations, the latter being strongly red-shifted.[11] For the high-aspect ratio spheroid, we also observe a quadrupolar LSP resonance around 700 nm.[36] When one ignores this higher-order resonance, the ratio $\eta(\lambda)$ remains for all shapes very close to, but always smaller than, the simple quasi-statics prediction; see Figure 4c. To be more precise, we observe that η for all shapes falls between that predicted by eq 9 for $d_{eq} = 60$ nm (the actual size) and $d_{eq} = 54$ nm (10% less). In other words, if we use the simple expression, eq 9, to determine the NP volume, the equivalent diameter is

https://dx.doi.org/10.1021/acsnano.0c08431
ACS Nano 2020, 14, 17597–17605

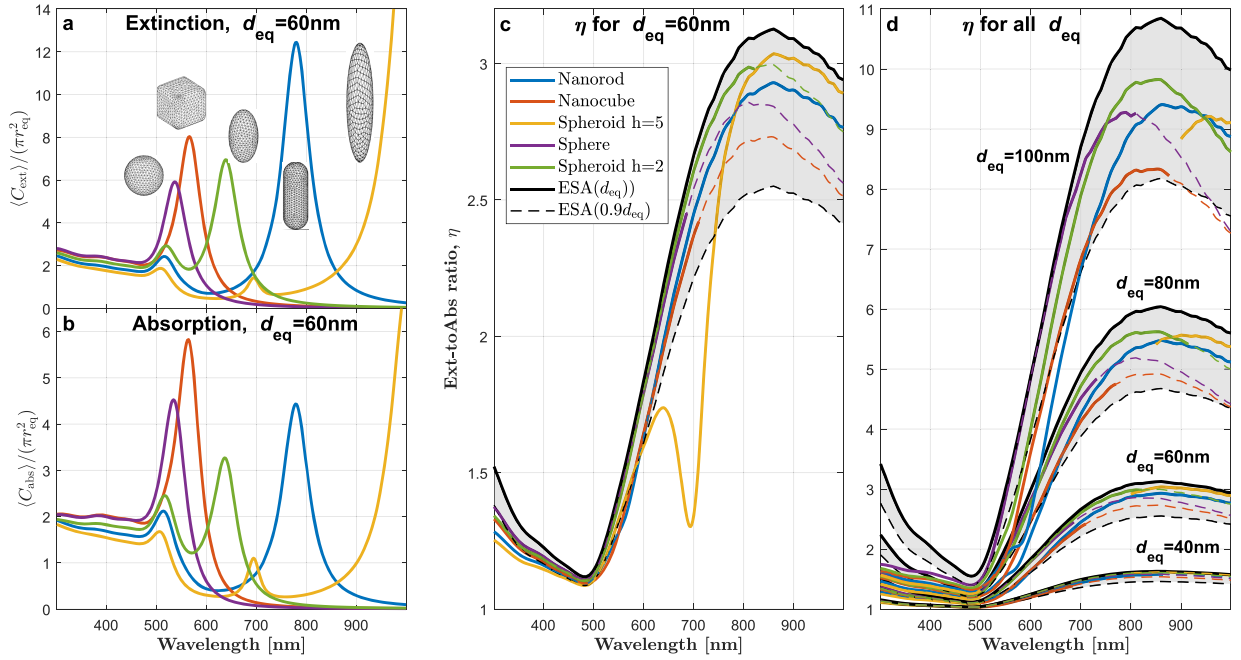

Figure 4. Calculated extinction coefficient (a), absorption coefficient (b), and extinction-to-absorption ratio η (c, d) spectra for gold NPs of various shapes: sphere, prolate spheroids of aspect ratio h = 2 and h = 5, nanorod with rounded ends (h = 3), and nanocube with rounded edges. In panels a−c, all NPs have the same volume corresponding to a sphere of equivalent diameter d_{eq} = 60 nm. The dependence on d_{eq} is studied in panel d, where the graphs for the spheroid with h = 5 are omitted in the spectral region of the quadrupolar resonance for clarity. In panels c and d, dashed lines indicate the region where the absorption spectrum is small (less than 1/50 of its maximum), as these would be difficult to measure experimentally. Note that the small oscillations/noise are due to imperfections/discretization of the dielectric function data.

overestimated by approx 5%, and with that small correction, it should be correct within ±5% *for any particle shape*. One small caveat is that this is not true at wavelengths where quadrupolar (or higher order) resonances dominate, as evident for example in the case of the spheroid of aspect ratio h = 5. In such situations, the method should only be applied around the dipolar (most red-shifted) plasmon resonance (above 800 nm for this spheroid).

While Figure 4c demonstrates that this method works for a fixed size d_{eq} = 60 nm, we investigate in Figure 4d the size dependence. The quadrupolar region of the more elongated spheroid was removed for clarity. At smaller sizes (40 nm diameter for example), the shape independence and agreement with eq 9 become even better, as expected given that it relies on the quasi-statics approximation valid in the limit of small sizes. For larger sizes, more spread is observed in η, but at d_{eq} = 100 nm, the predictions remain between that of eq 9 for d_{eq} = 100 nm (the correct value) and d_{eq} = 90 nm (10% less). Thus, we expect the method to work up to around d_{eq} = 100 nm; beyond that, the quasi-statics approximation is no longer expected to be valid and more deviations are observed. Figure 4d also clearly shows again the strong sensitivity of η to size, here independently of shape up to $d_{eq} \approx$ 100 nm.

Using η to Infer the Dielectric Function of Gold Nanoparticles. We now return to the issue of the choice of dielectric function. The optical properties of gold may vary depending on the quality and preparation methods of the NPs or films.[30,38] Different dielectric functions have been proposed, some of which are plotted in Figure 5a,b: Experimental data from Johnson and Christy's 1972 ellipsometric measurements[31] (labeled JC), values measured for an optimized preparation method of gold[32] (2015), an analytical model for gold−silver alloys from ref 33 (2014), and a variety of experimentally measured values depending on the gold film preparation method from ref 30, namely, for template-stripped (2012TS), a single crystal sample (2012SC), and evaporated (2012EV) gold. While the dielectric function for gold films and single crystals can be measured experimentally, albeit with some complications, doing so for AuNPs is even more difficult, and the choice of dielectric function used for the comparison with the theory is usually arbitrary. However, as shown in Figure 1e, different choices of dielectric function lead to significantly different NP size estimates when inferred from the extinction spectrum only.

In contrast, because η is not sensitive to shape or to the position of the plasmon resonance, it provides a fairly constrained experimental test of the theory over the entire spectral range where it can be measured, typically from 400 to 600 nm for gold nanospheres. We show that this can be exploited to make inferences on the dielectric function. In fact, for small particles, eq 9 in principle provides a direct expression for $\mathrm{Im}(\epsilon_M/(\epsilon - \epsilon_M))$ in terms of V, λ, and $\eta(\lambda) - 1$. In practice, however, measuring $\eta - 1$ accurately for the smallest particles is difficult as η is too close to 1. It is therefore better to use intermediate-size particles (typically 50−80 nm), but eq 9 is then not accurate enough to make inferences on the dielectric function. For spherical particles, we can use the Mie theory instead, especially given that small shape imperfections should have negligible effects given the shape independence of η. According to our earlier discussion and Figure 3, the size distribution may have a small effect on the wavelength dependence. As this is likely comparable to the dielectric function effect, it is important to account for it in our calculations, which can be done by measuring the size

https://dx.doi.org/10.1021/acsnano.0c08431
ACS Nano 2020, 14, 17597−17605

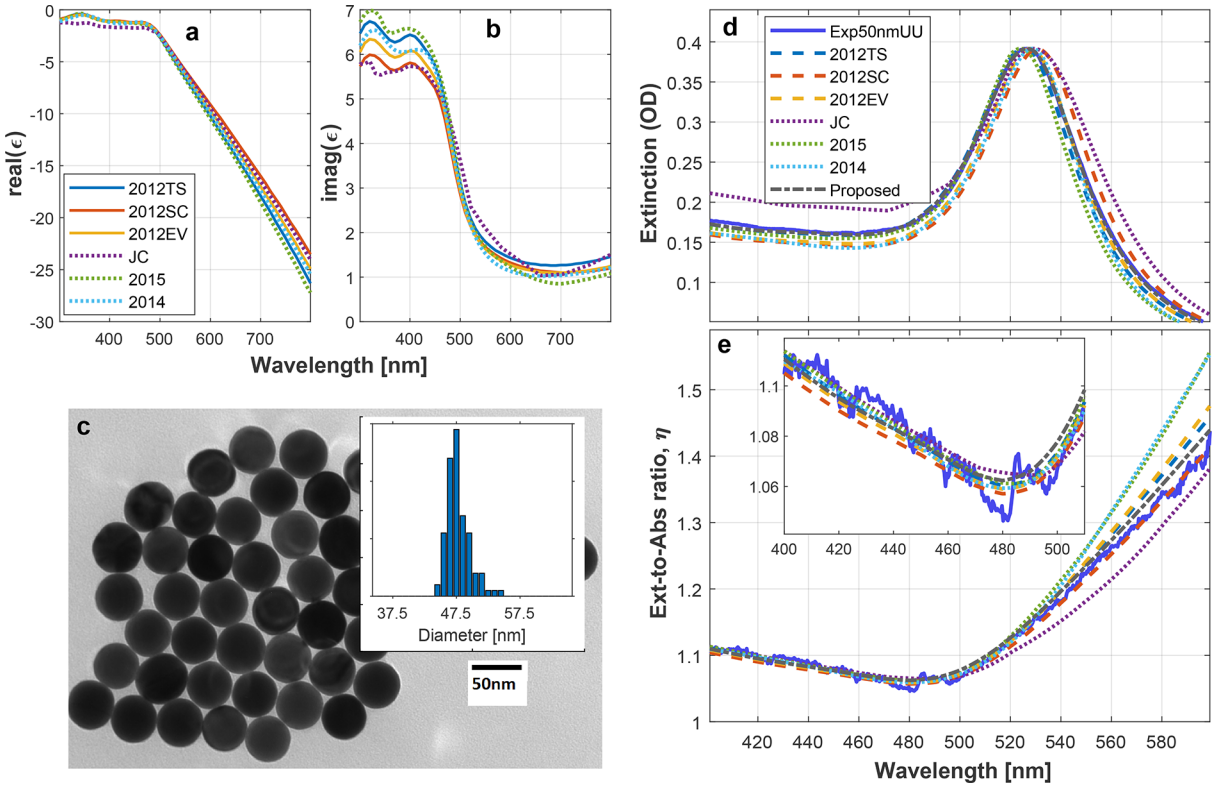

Figure 5. Effect of the dielectric function. Comparison of different data sets for the real (a) and imaginary (b) part of the dielectric: Template-stripped (2012TS), single crystal (2012SC), and evaporated (2012EV) from ref 30, Johnson and Christy (JC),[31] and two other recent measurements from ref 32 (2015) and from ref 33 (2014). (c) TEM and size distribution for the ultra-uniform AuNPs of diameter 47.8 ± 1.8 nm used for this measurement. Experimental results for the extinction (d) and extinction-to-absorption ratio (e) are compared to the Mie theory for the different dielectric function models. The proposed model corresponds to the 2012SC model with 0.3 subtracted from the real part.

distribution with TEM. To further minimize any possible effect of the size distribution, we here use ultra-uniform 50 nm gold nanospheres. From TEM images, these exhibit an ultra-narrow size distribution centered at 47.8 nm with a standard deviation of only 1.8 nm; see Figures 5c and S5. The Mie theory was used, accounting for this measured size distribution, with various models of the gold dielectric function. The predictions are compared to the experimentally measured extinction and absorption spectra, as well as their ratio, in Figure 5d,e. We obtain a range of extinction spectra with small peak shifts (Figure 5d). These shifts are primarily determined by the exact value of the dielectric function at the plasmon resonance of around 525 nm, so extinction cannot be used to discriminate strongly between these dielectric functions over the full wavelength range.

The situation is different for η (Figure 5e): $\eta(\lambda)$ shows variations across the spectral region for different dielectric functions, and these cannot be explained simply by small changes in size or shape. It is clear from Figure 5e that the predictions using dielectric functions labeled JC, 2014, and 2015 disagree with our experimental data. Those reported in ref 30 (2012TS, 2012EV, and 2012SC) appear to provide the closest agreement. From a single measurement, it is difficult to argue in favor of or against one of these three data sets. There is a hint that SC data provide the closest fit to $\eta(\lambda)$ since the other two tend to overestimate η slightly above ≈550 nm. The same consistent picture is in fact observed for all the other NP sizes considered before (50−80 nm citrate AuNPs, not ultra-uniform) as shown in Figures S1−S4. Note that all these predictions have no free parameters, as the size distribution is directly taken from the TEM measurements of 100 particles as shown in Figures S5−S9. These additional fits also favor the SC data as the most accurate for η predictions. The SC data however also consistently predict an extinction spectrum that is slightly red-shifted compared to the experiments, which is clearly not satisfactory. The EV and TS data are better in this respect. We propose an even better alternative: to slightly modify the SC data to correct the extinction shift without affecting η too much. A simple way to achieve this, which does not compromise the Kramers-Krönig consistency in the wavelength range of interest, is to subtract a small constant from the real part of ϵ. We found that taking

$$\mathrm{Re}(\epsilon_{\mathrm{New}}) = \mathrm{Re}(\epsilon_{\mathrm{SC}}) - 0.3$$
$$\mathrm{Im}(\epsilon_{\mathrm{New}}) = \mathrm{Im}(\epsilon_{\mathrm{SC}}) \quad (10)$$

achieved the required shift in extinction without affecting η too much. The corresponding predictions are shown in Figures 5d,e and S1−S4. We speculate that such an offset could be the result of surface charges or surface roughness slightly affecting the plasma frequency,[39] but given the magnitude of the effect, other alternatives would result in comparable corrections, for example, if we accounted for the thin solvated shell surrounding the NPs and affecting the local refractive index. This aspect would require further investigations. In any case, this proposed dielectric function results in an extremely good agreement for both extinction and η for the ultra-uniform 50 nm AuNPs. It should be emphasized that it is highly

https://dx.doi.org/10.1021/acsnano.0c08431
ACS Nano 2020, 14, 17597−17605

uncommon to observe such a good agreement over the full spectral range for the extinction spectrum for gold nanospheres, which we attribute here to the ultra-low shape and size polydispersity, as discussed previously for nanorods.[22] The same agreement is not observed for standard NPs (see Figures S1−S4), especially in the region of 400−500 nm, which confirms our recent study showing that this region is particularly affected by shape polydispersity.[23] $\eta(\lambda)$ is much less sensitive to this problem, which only appears for the larger size NPs (70 and 80 nm) and even then remains very small.

CONCLUSIONS

Using a combination of experiments and theory, we have demonstrated that the extinction-to-absorption ratio η is an extremely powerful tool to determine the volume of gold NPs in the range of 25−150 nm (volume-equivalent diameter). If the shape is well-defined, the NP dimensions can therefore be deduced. Moreover, this ratio becomes independent of shape in the regime where the quasi-static/dipolar approximation is valid, *i.e.*, when the particles are small enough, typically less than 100 nm, and in the spectral region away from the quadrupole or higher order resonance peaks. Note that these constraints still encompass the majority of NPs used in biological and chemical applications. We believe the conclusions of this work will readily extend to other types of metallic NPs, such as silver NPs. The use of the ratio η to determine NP size is a significant improvement compared to solely using extinction spectroscopy and can be implemented relatively simply, for example, using an integrating sphere-based transmission setup. The benefits of the method therefore greatly outweigh the additional experimental effort and will enable the routine accurate size characterization of the nanoparticles.

An equally interesting, more fundamental, aspect of this work is that the shape insensitivity of η provides very strong constraints when comparing its spectrum to theoretical predictions. By measuring ultra-uniform gold nanospheres characterized with TEM, we were able to further reduce any uncertainty in size distribution to the point where the only remaining "free" parameter in the theoretical predictions is the dielectric function of gold. This allowed us to discriminate between various dielectric function data sets reported in the literature, thereby tackling a long-standing challenge in plasmonics research. Three data sets are clearly incompatible with our results, including the commonly used Johnson and Christy data.[31] The three data sets that are favored by our analysis are all from the same publication[30] and correspond to three different preparation procedures. This suggests that the problem with the other three nonfavored sets lies in systematic errors in the measurements rather than in different sample preparations. An accurate measurement of the dielectric function of metal is indeed notoriously difficult because of the complications due to the metal/dielectric interface. Among the three favored data sets, the experimental results appeared to agree most with the single crystal data, which suggests that chemically synthesized gold NPs exhibit a relatively good crystallinity.

METHODS

Gold Nanoparticles. 50 nm Ultra-Uniform PEG_{12}-carboxylic-acid-coated gold nanopsheres and 50, 60, 70, and 80 nm citrate-stabilized gold nanospheres were obtained from NanoComposix (USA). TEM images (see Figures S5−S9) and size distributions were provided by NanoComposix. The size distributions were inferred from the TEM images of 100 particles and are shown in Figures 5c and S1b−S4b. The corresponding mean and standard deviations are 47.8 ± 1.8 nm (ultra-uniform) and 49 ± 5, 63 ± 7, 70 ± 8, and 78 ± 9 nm, respectively.

Absorption/Extinction Measurements. The optical properties of the AuNP solutions were measured using the CloudSpec-UV instrument from Marama Labs (New Zealand). This instrument simultaneously collects the extinction and absorption spectra of the sample using Xenon flash lamp excitation. The absorption measurement uses an integrating sphere to remove any scattering interference from the transmission.[24−26,28,29] The latter can be calibrated to return to the absolute absorption,[23,26,29] with both extinction and absorption then given in units of $[cm^{-1}]$, *i.e.*, in optical density normalized to a 1 cm path length. The scattering spectrum is, therefore, obtained from the difference of the two. Note that this method is different from diffuse reflectance/transmittance spectroscopy where the scattering or effective-scattering spectrum is directly inferred. Like standard UV−vis spectroscopy, this method is therefore not affected by the inner filter effect that may affect fluorescence and other methods. The instrument was recalibrated before the measurements, and the stock NP colloidal suspension was diluted by a factor of 4 for all measurements. The same cuvette is used for the sample and reference (water). The main source of error in the calculation of η comes from the reference (baseline) in the extinction spectra and is estimated to be of the order of a few 10^{-3} OD. Because the absorption measurement benefits from a path length enhancement in the integrating sphere, it is less sensitive to this problem. The fixed noise observed in the spectra of η (for example at 480 nm) corresponds to xenon lamp peaks and is the result of slight nonlinearities (of the order of 0.1%) in the detector response. These tiny glitches become apparent in the ratio because of the scale at which it is plotted.

Electromagnetic Calculations. Mie theory calculations were performed using the SPlaC package.[11,40] New routines were written to account for the size distribution. The optical properties of the spheroidal AuNPs were computed using SMARTIES,[41] a Matlab implementation of the *T*-Matrix method including recently developed improved algorithms especially developed for spheroidal NPs.[36,41,42] An estimate of the accuracy of the results is returned by the computation, and high accuracy (comparable to the Mie theory, better than 10^{-12})[42] is achieved for all the examples considered here. The *T*-matrix method is particularly suited to calculate orientation-averaged cross sections. For other nonspherical particles, namely, the gold nanorods (AuNRs) and the gold nanocubes, the surface integral equation formalism was used.[43,44] We have used an implementation specially developed (and tested) for plasmonics and in particular plasmonic metallic NPs.[45] Accuracies in the cross sections better than 1% are expected with the mesh we used. The nanorod was modeled as a cylinder with hemispherical caps with an overall height-to-width ratio of 3. The nanocube's edges were rounded to represent more realistic particles.[23] Exact volumes were calculated directly from the meshes. The orientation averaging was performed using a Gaussian quadrature of 91 incident angles and using the fact that these shapes had a symmetry of revolution with two perpendicular polarizations for each incidence. In all the calculations, the wavelength-dependent refractive index for water was taken from ref 46. Different dielectric functions for gold were used as discussed in the text. Linear interpolations were used to obtain wavelength-dependent dielectric functions from discrete data.

ASSOCIATED CONTENT

Supporting Information

The Supporting Information is available free of charge at https://pubs.acs.org/doi/10.1021/acsnano.0c08431.

Equivalent to Figure 5 for 50, 60, 70, and 80 nm citrate-reduced gold NPs; TEM images of the gold NP solutions used in this work (PDF)

https://dx.doi.org/10.1021/acsnano.0c08431
ACS Nano 2020, 14, 17597−17605

AUTHOR INFORMATION

Corresponding Author

Eric C. Le Ru − *The MacDiarmid Institute for Advanced Materials and Nanotechnology, School of Chemical and Physical Sciences, Victoria University of Wellington, Wellington 6140, New Zealand;* orcid.org/0000-0002-3052-9947; Email: eric.leru@vuw.ac.nz

Authors

Aleksa Djorović − *The MacDiarmid Institute for Advanced Materials and Nanotechnology, School of Chemical and Physical Sciences, Victoria University of Wellington, Wellington 6140, New Zealand;* orcid.org/0000-0002-0809-4887

Steven J. Oldenburg − *nanoComposix, San Diego, California 92111, United States*

Johan Grand − *The MacDiarmid Institute for Advanced Materials and Nanotechnology, School of Chemical and Physical Sciences, Victoria University of Wellington, Wellington 6140, New Zealand; Université de Paris, ITODYS, CNRS, UMR 7086, F-75013 Paris, France;* orcid.org/0000-0001-6920-5184

Complete contact information is available at: https://pubs.acs.org/10.1021/acsnano.0c08431

Notes

The authors declare the following competing financial interest(s): The instrument used for the measurements discussed in this manuscript was developed and is commercialized by Marama Laboratories Ltd., a start-up company that was spun out from E.C.L.R.'s research. E.C.L.R. therefore has a small share in this company. Moreover, S.J.O. is CEO and co-founder of nanoComposix, which manufactures and commercializes the nanoparticles used in this work.

ACKNOWLEDGMENTS

The authors thank Marama Labs Ltd. (New Zealand) for providing us early access to an earlier prototype of their instrument and Nanocomposix Ltd. (USA) for providing us with the gold NP solutions used in this study. E.C.L.R. acknowledges the support of the Royal Society Te Apārangi (New Zealand) through a Marsden Grant and of the MacDiarmid Institute for Advanced Materials and Nanotechnology.

REFERENCES

(1) Hutter, E.; Fendler, J. H. Exploitation of Localized Surface Plasmon Resonance. *Adv. Mater.* **2004**, *16*, 1685−1706.

(2) Amendola, V.; Pilot, R.; Frasconi, M.; Maragò, O. M.; Iatì, M. A. Surface Plasmon Resonance in Gold Nanoparticles: A Review. *J. Phys.: Condens. Matter* **2017**, *29*, 203002.

(3) Tshikhudo, T.; Wang, Z.; Brust, M. Biocompatible Gold Nanoparticles. *Mater. Sci. Technol.* **2004**, *20*, 980−984.

(4) Elahi, N.; Kamali, M.; Baghersad, M. H. Recent Biomedical Applications of Gold Nanoparticles: A Review. *Talanta* **2018**, *184*, 537−556.

(5) Alexandridis, P. Gold Nanoparticle Synthesis, Morphology Control, and Stabilization Facilitated by Functional Polymers. *Chem. Eng. Technol.* **2011**, *34*, 15−28.

(6) Wang, Z.; Ma, L. Gold Nanoparticle Probes. *Coord. Chem. Rev.* **2009**, *253*, 1607−1618.

(7) Giasuddin, A.; Jhuma, K.; Haq, A. M. Use of Gold Nanoparticles in Diagnostics, Surgery and Medicine: A Review. *Bangladesh J. Med. Biochem.* **2013**, *5*, 56−60.

(8) Haiss, W.; Thanh, N. T.; Aveyard, J.; Fernig, D. G. Determination of Size and Concentration of Gold Nanoparticles from Uv- Vis Spectra. *Anal. Chem.* **2007**, *79*, 4215−4221.

(9) Cheng, Y.; Samia, A. C.; Meyers, J. D.; Panagopoulos, I.; Fei, B.; Burda, C. Highly Efficient Drug Delivery with Gold Nanoparticle Vectors for *in Vivo* Photodynamic Therapy of Cancer. *J. Am. Chem. Soc.* **2008**, *130*, 10643−10647.

(10) Turner, M.; Golovko, V. B.; Vaughan, O. P.; Abdulkin, P.; Berenguer-Murcia, A.; Tikhov, M. S.; Johnson, B. F.; Lambert, R. M. Selective Oxidation with Dioxygen by Gold Nanoparticle Catalysts Derived from 55-Atom Clusters. *Nature* **2008**, *454*, 981−983.

(11) Le Ru, E. C.; Etchegoin, P. *Principles of Surface-Enhanced Raman Spectroscopy: And Related Plasmonic Effects*; Elsevier: Amsterdam, 2009.

(12) Willets, K. A.; Van Duyne, R. P. Localized Surface Plasmon Resonance Spectroscopy and Sensing. *Annu. Rev. Phys. Chem.* **2007**, *58*, 267−297.

(13) Chithrani, B. D.; Ghazani, A. A.; Chan, W. C. W. Determining the Size and Shape Dependence of Gold Nanoparticle Uptake into Mammalian Cells. *Nano Lett.* **2006**, *6*, 662−668.

(14) Amendola, V.; Meneghetti, M. Size Evaluation of Gold Nanoparticles by UV- Vis Spectroscopy. *J. Phys. Chem. C* **2009**, *113*, 4277−4285.

(15) Schaffer, B.; Hohenester, U.; Trügler, A.; Hofer, F. High-Resolution Surface Plasmon Imaging of Gold Nanoparticles by Energy-Filtered Transmission Electron Microscopy. *Phys. Rev. B: Condens. Matter Mater. Phys.* **2009**, *79*, No. 041401.

(16) Azubel, M.; Koivisto, J.; Malola, S.; Bushnell, D.; Hura, G. L.; Koh, A. L.; Tsunoyama, H.; Tsukuda, T.; Pettersson, M.; Häkkinen, H.; Kornberg, R. D. Electron Microscopy of Gold Nanoparticles at Atomic Resolution. *Science* **2014**, *345*, 909−912.

(17) Berne, B. J.; Pecora, R. *Dynamic Light Scattering: With Applications to Chemistry, Biology, and Physics*; Dover Publications: New York, 2000.

(18) Khlebtsov, B. N.; Khlebtsov, N. G. On the Measurement of Gold Nanoparticle Sizes by the Dynamic Light Scattering Method. *Colloid J.* **2011**, *73*, 118−127.

(19) Zheng, T.; Bott, S.; Huo, Q. Techniques for Accurate Sizing of Gold Nanoparticles Using Dynamic Light Scattering with Particular Application to Chemical and Biological Sensing Based on Aggregate Formation. *ACS Appl. Mater. Interfaces* **2016**, *8*, 21585−21594.

(20) Hole, P.; Sillence, K.; Hannell, C.; Maguire, C. M.; Roesslein, M.; Suarez, G.; Capracotta, S.; Magdolenova, Z.; Horev-Azaria, L.; Dybowska, A.; Cooke, L.; Haase, A.; Contal, S.; Manø, S.; Vennemann, A.; Sauvain, J.-J.; Staunton, K. C.; Anguissola, S.; Luch, A.; Dusinska, M.; et al. Interlaboratory Comparison of Size Measurements on Nanoparticles Using Nanoparticle Tracking Analysis (NTA). *J. Nanopart. Res.* **2013**, *15*, 2101.

(21) Arancon, R. A. D.; Lin, S. H. T.; Chen, G.; Lin, C. S. K.; Lai, J.; Xu, G.; Luque, R. Nanoparticle Tracking Analysis of Gold Nanomaterials Stabilized by Various Capping Agents. *RSC Adv.* **2014**, *4*, 17114−17119.

(22) González-Rubio, G.; Díaz-Núñez, P.; Rivera, A.; Prada, A.; Tardajos, G.; González-Izquierdo, J.; Bañares, L.; Llombart, P.; Macdowell, L. G.; Alcolea Palafox, M.; Liz-Marzán, L. M.; Peña-Rodríguez, O.; Guerrero-Martínez, A. Femtosecond Laser Reshaping Yields Gold Nanorods with Ultranarrow Surface Plasmon Resonances. *Science* **2017**, *358*, 640−644.

(23) Grand, J.; Auguié, B.; Le Ru, E. C. Combined Extinction and Absorption UV−Visible Spectroscopy as a Method for Revealing Shape Imperfections of Metallic Nanoparticles. *Anal. Chem.* **2019**, *91*, 14639−14648.

(24) Nelson, N. B.; Prézelin, B. B. Calibration of an Integrating Sphere for Determining the Absorption Coefficient of Scattering Suspensions. *Appl. Opt.* **1993**, *32*, 6710−6717.

(25) Evanoff, D. D.; Chumanov, G. Size-Controlled Synthesis of Nanoparticles. 2. Measurement of Extinction, Scattering, and Absorption Cross Sections. *J. Phys. Chem. B* **2004**, *108*, 13957−13962.
(26) Jávorfi, T.; Erostyák, J.; Gál, J.; Buzády, A.; Menczel, L.; Garab, G.; Naqvi, K. R. Quantitative Spectrophotometry Using Integrating Cavities. *J. Photochem. Photobiol., B* **2006**, *82*, 127−131.
(27) Gaigalas, A. K.; He, H.-J.; Wang, L. Measurement of Absorption and Scattering with an Integrating Sphere Detector: Application to Microalgae. *J. Res. Natl. Inst. Stand. Technol.* **2009**, *114*, 69−81.
(28) Darby, B. L.; Auguié, B.; Meyer, M.; Pantoja, A. E.; Le Ru, E. C. Modified Optical Absorption of Molecules on Metallic Nanoparticles at Sub-Monolayer Coverage. *Nat. Photonics* **2016**, *10*, 40.
(29) Villanueva, Y.; Veenstra, C.; Steenbergen, W. Measuring Absorption Coefficient of Scattering Liquids Using a Tube Inside an Integrating Sphere. *Appl. Opt.* **2016**, *55*, 3030−3038.
(30) Olmon, R. L.; Slovick, B.; Johnson, T. W.; Shelton, D.; Oh, S.-H.; Boreman, G. D.; Raschke, M. B. Optical Dielectric Function of Gold. *Phys. Rev. B: Condens. Matter Mater. Phys.* **2012**, *86*, 235147.
(31) Johnson, P. B.; Christy, R.-W. Optical Constants of the Noble Metals. *Phys. Rev. B* **1972**, *6*, 4370.
(32) McPeak, K. M.; Jayanti, S. V.; Kress, S. J.; Meyer, S.; Iotti, S.; Rossinelli, A.; Norris, D. J. Plasmonic Films Can Easily Be Better: Rules and Recipes. *ACS Photonics* **2015**, *2*, 326−333.
(33) Rioux, D.; Vallières, S.; Besner, S.; Muñoz, P.; Mazur, E.; Meunier, M. An Analytic Model for the Dielectric Function of Au, Ag, and Their Alloys. *Adv. Opt. Mater.* **2014**, *2*, 176−182.
(34) Etchegoin, P. G.; Le Ru, E.; Meyer, M. An Analytic Model for the Optical Properties of Gold. *J. Chem. Phys.* **2006**, *125*, 164705.
(35) Il'in, V. B.; Farafonov, V. G. Rayleigh Approximation for Axisymmetric Scatterers. *Opt. Lett.* **2011**, *36*, 4080−4082.
(36) Majic, M.; Pratley, L.; Schebarchov, D.; Somerville, W. R.; Auguié, B.; Le Ru, E. C. Approximate T-Matrix and Optical Properties of Spheroidal Particles to Third Order with Respect to Size Parameter. *Phys. Rev. A: At., Mol., Opt. Phys.* **2019**, *99*, No. 013853.
(37) Le Ru, E. C.; Somerville, W. R.; Auguié, B. Radiative Correction in Approximate Treatments of Electromagnetic Scattering by Point and Body Scatterers. *Phys. Rev. A: At., Mol., Opt. Phys.* **2013**, *87*, No. 012504.
(38) Khan, M. A.; Zhu, Y.; Yao, Y.; Zhang, P.; Agrawal, A.; Reece, P. J. Impact of Metal Crystallinity-Related Morphologies on the Sensing Performance of Plasmonic Nanohole Arrays. *Nanoscale* **2020**, *12*, 7577−7585.
(39) Trügler, A.; Tinguely, J.-C.; Krenn, J. R.; Hohenau, A.; Hohenester, U. Influence of Surface Roughness on the Optical Properties of Plasmonic Nanoparticles. *Phys. Rev. B: Condens. Matter Mater. Phys.* **2011**, *83*, No. 081412.
(40) Le Ru, E. C.; Etchegoin, P. G. *SERS and Plasmonics Codes (SPlaC)*; Matlab codes freely available from https://www.wgtn.ac.nz/scps/research/research-groups/raman-lab/numerical-tools/sers-and-plasmonics-codes (accessed 2020-12-01).
(41) Somerville, W.; Auguié, B.; Le Ru, E. SMARTIES: User-Friendly Codes for Fast and Accurate Calculations of Light Scattering by Spheroids. *J. Quant. Spectrosc. Radiat. Transfer* **2016**, *174*, 39−55.
(42) Somerville, W.; Auguié, B.; Le Ru, E. Accurate and Convergent T-Matrix Calculations of Light Scattering by Spheroids. *J. Quant. Spectrosc. Radiat. Transfer* **2015**, *160*, 29−35.
(43) Kern, A. M.; Martin, O. J. Surface Integral Formulation for 3D Simulations of Plasmonic and High Permittivity Nanostructures. *J. Opt. Soc. Am. A* **2009**, *26*, 732−740.
(44) Kern, A. M.; Martin, O. J. Excitation and Reemission of Molecules near Realistic Plasmonic Nanostructures. *Nano Lett.* **2011**, *11*, 482−487.
(45) Raziman, T.; Somerville, W.; Martin, O. J.; Le Ru, E. Accuracy of Surface Integral Equation Matrix Elements in Plasmonic Calculations. *J. Opt. Soc. Am. B* **2015**, *32*, 485−492.
(46) Harvey, A. H.; Gallagher, J. S.; Sengers, J. L. Revised Formulation for the Refractive Index of Water and Steam as a Function of Wavelength, Temperature and Density. *J. Phys. Chem. Ref. Data* **1998**, *27*, 761−774.

https://dx.doi.org/10.1021/acsnano.0c08431
ACS Nano 2020, 14, 17597−17605

Supporting Information for "Extinction-to-Absorption Ratio for Sensitive Determination of the Size and Dielectric Function of Gold Nanoparticles"

Aleksa Djorović,[1] Steven J. Oldenburg,[2] Johan Grand,[1,3] and Eric C. Le Ru[1,*]

[1] *The MacDiarmid Institute for Advanced Materials and Nanotechnology, School of Chemical and Physical Sciences, Victoria University of Wellington, P.O. Box 600, Wellington 6140, New Zealand*

[2] *nanoComposix, 4878 Ronson Court Suite K, San Diego, CA 92111, USA*

[3] *Université de Paris, ITODYS, CNRS, UMR 7086, 15 rue J-A de Baïf, F-75013 Paris, France*

(Dated: November 18, 2020)

Supplementary Figures S1 to S9 are provided in the following.

* eric.leru@vuw.ac.nz

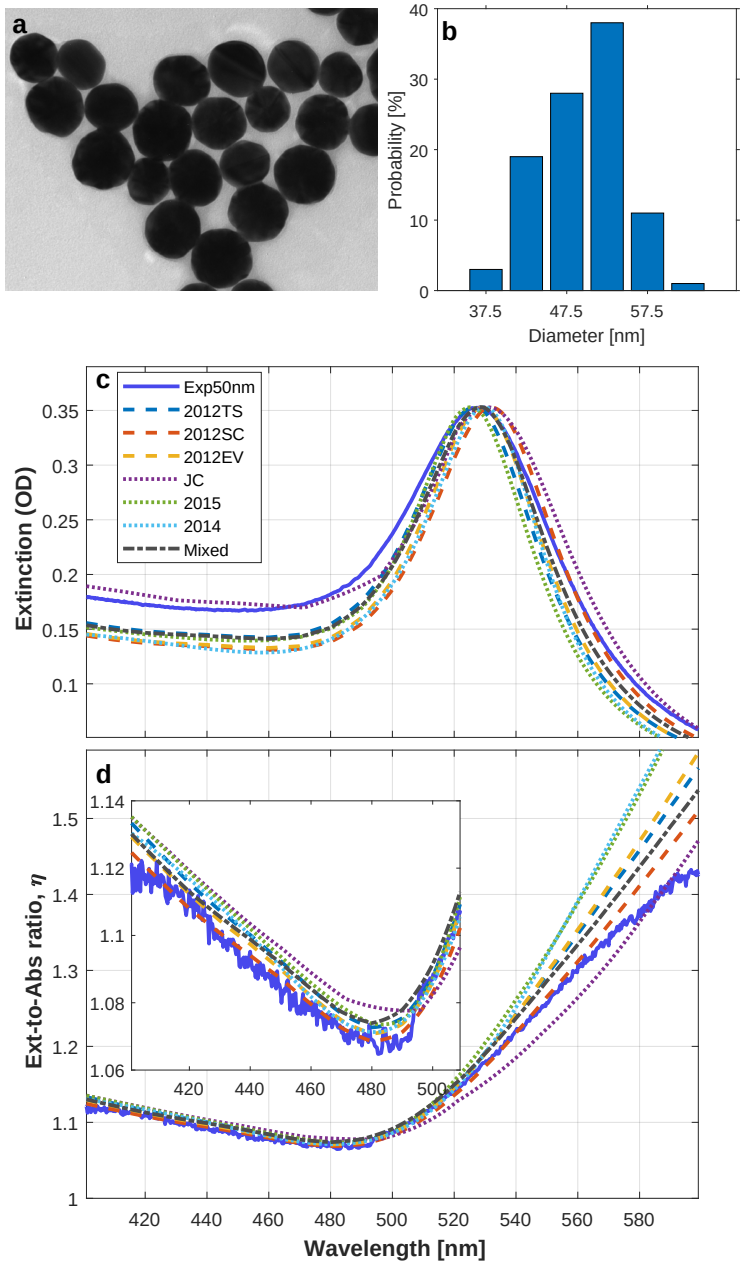

FIG. S1. Same as Fig. 5, but for the 50 nm citrate-reduced NPs.

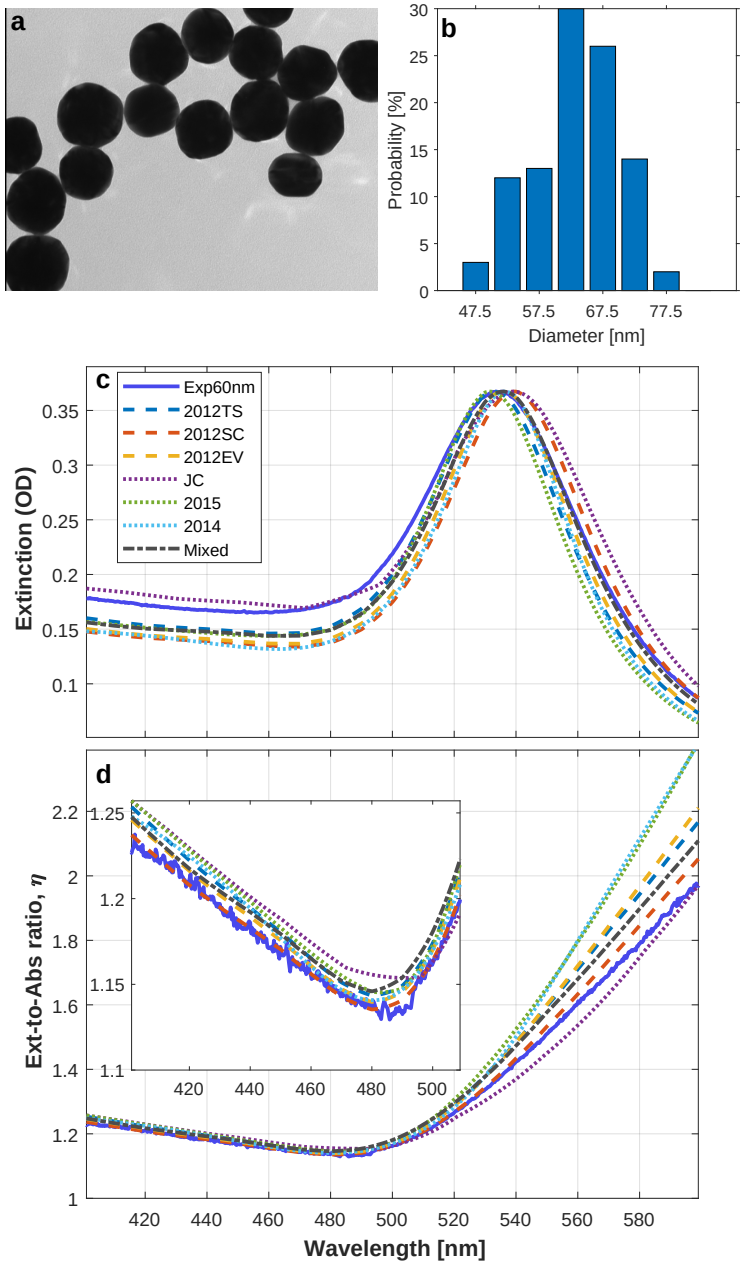

FIG. S2. Same as Fig. 5, but for the 60 nm citrate-reduced NPs.

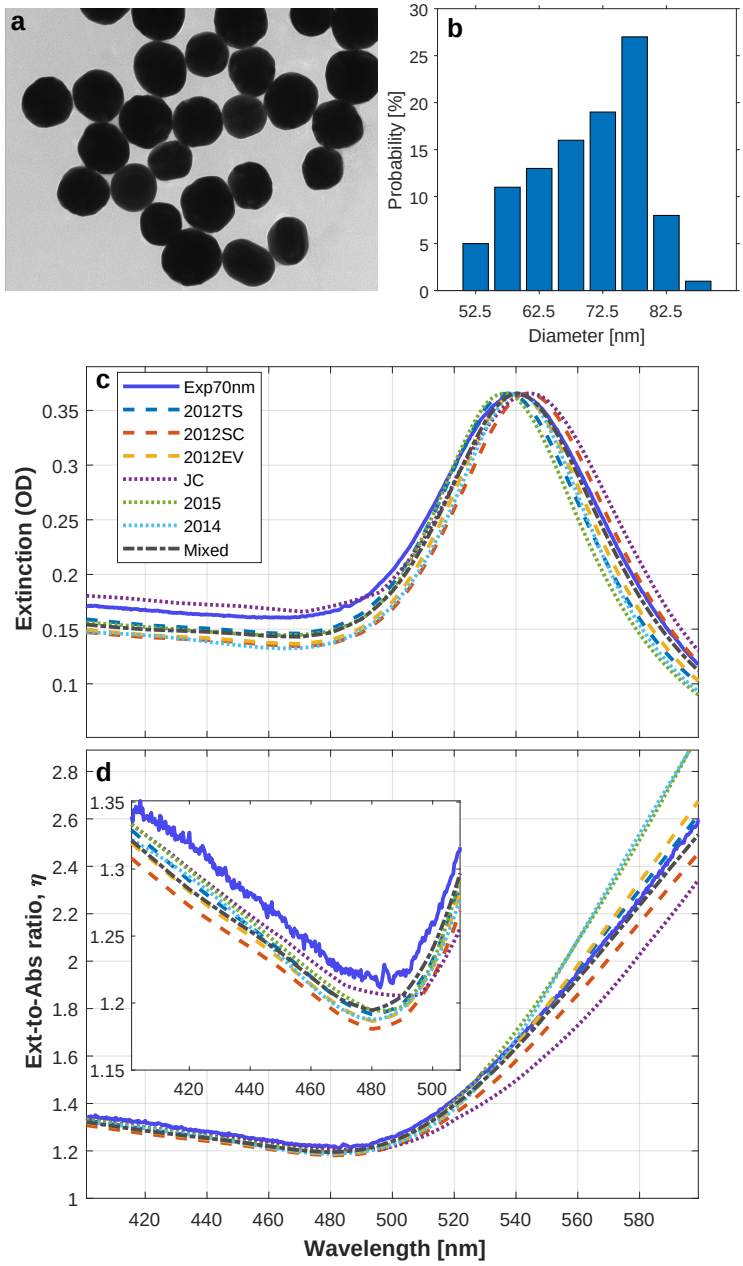

FIG. S3. Same as Fig. 5, but for the 70 nm citrate-reduced NPs.

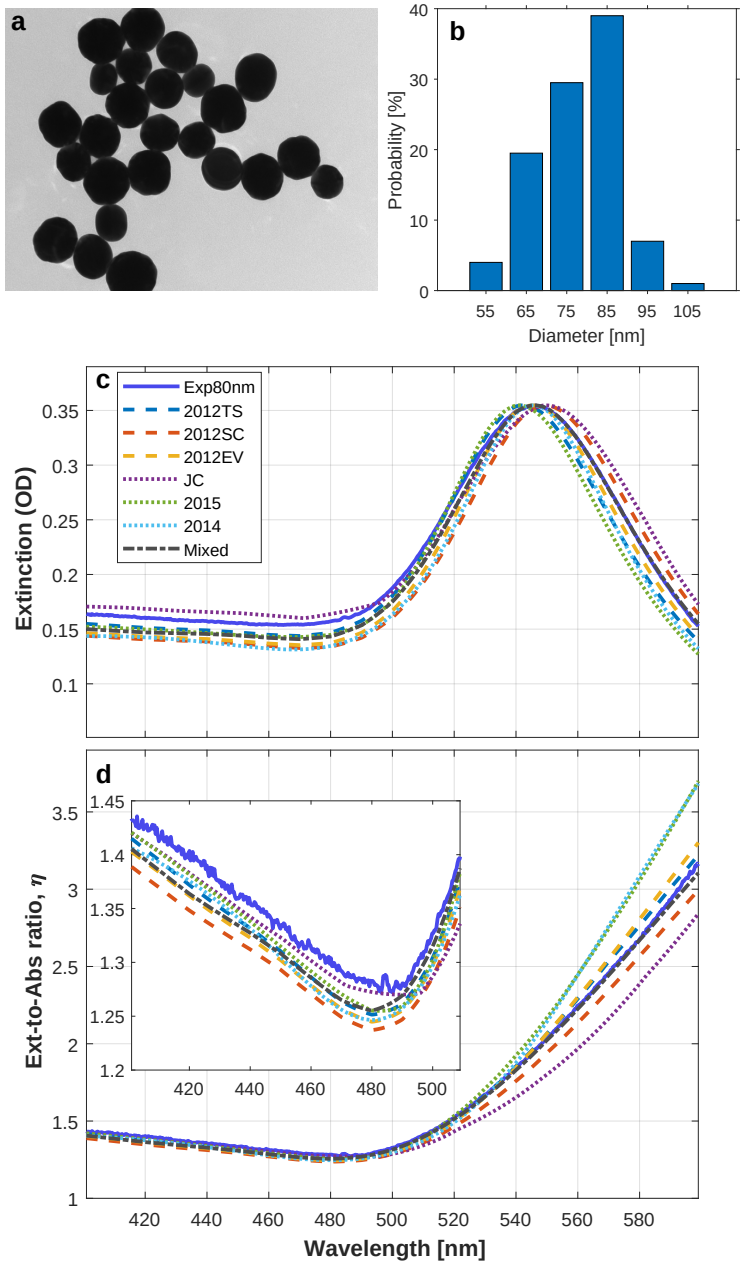

FIG. S4. Same as Fig. 5, but for the 80 nm citrate-reduced NPs.

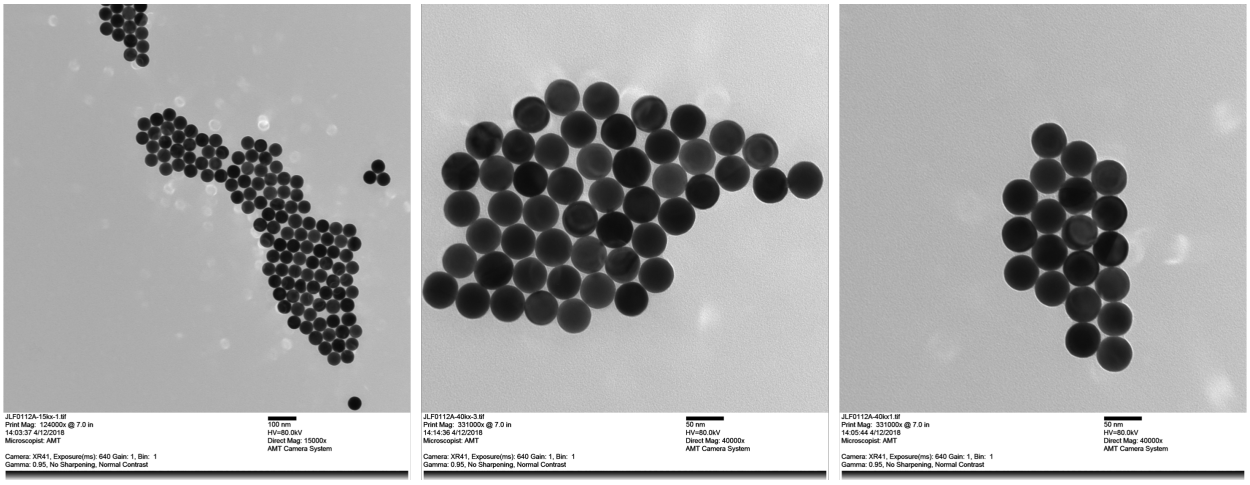

FIG. S5. TEM images of the 50 nm UltraUniform AuNPs.

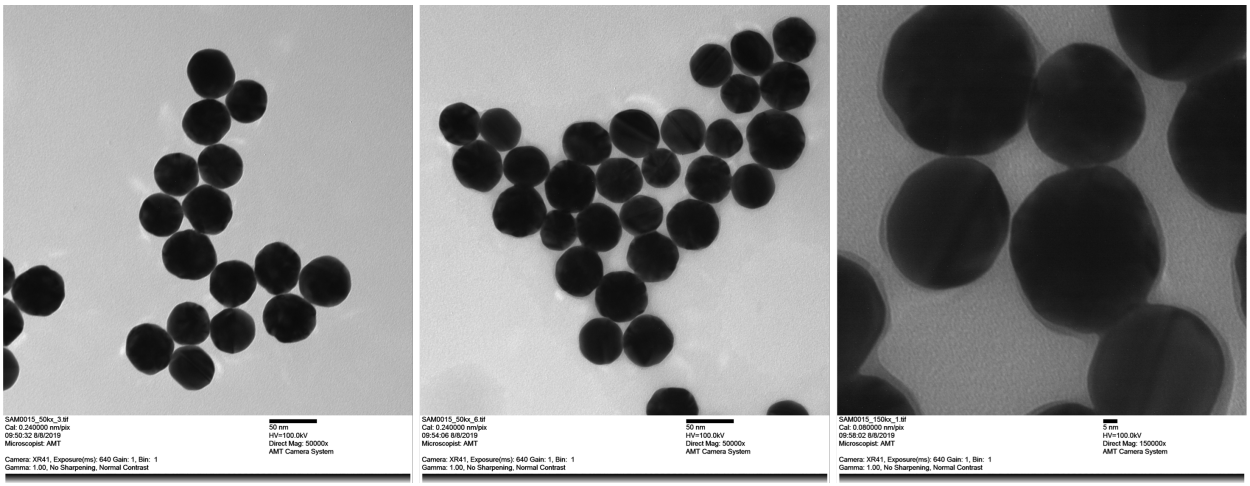

FIG. S6. TEM images of the 50 nm NanoXact AuNPs.

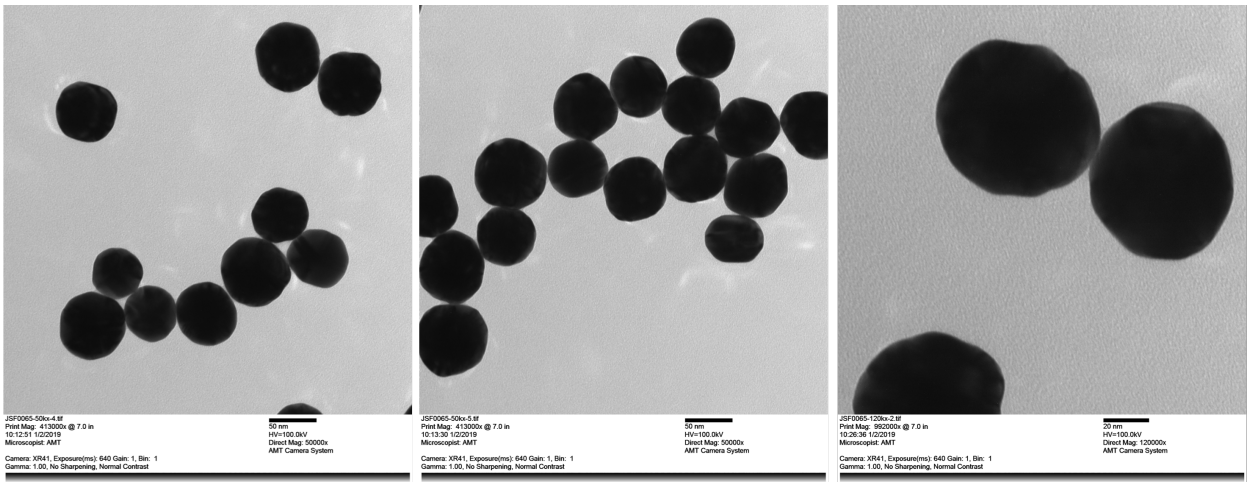

FIG. S7. TEM images of the 60 nm NanoXact AuNPs.

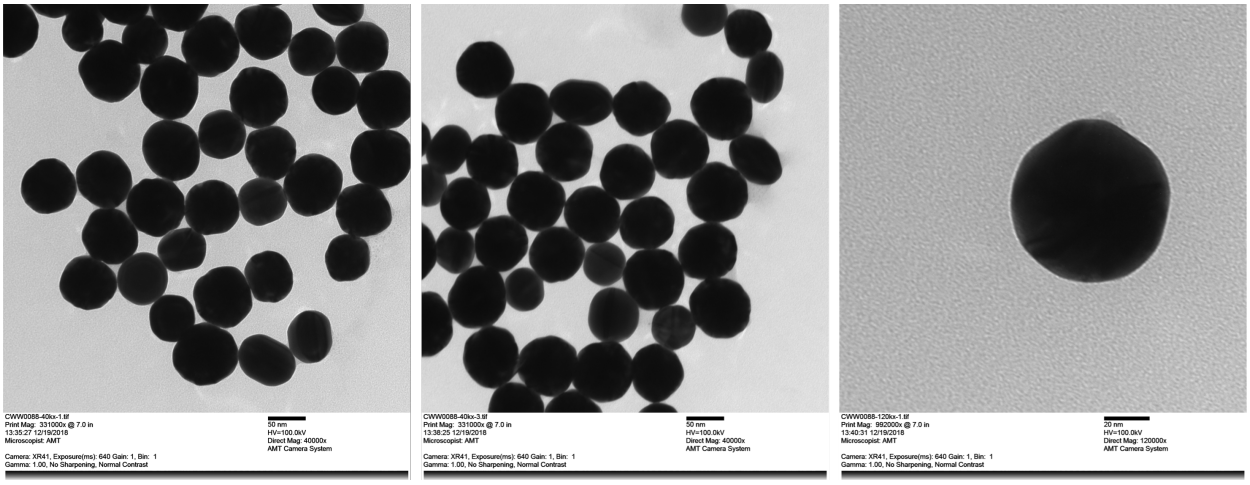

FIG. S8. TEM images of the 70 nm NanoXact AuNPs.

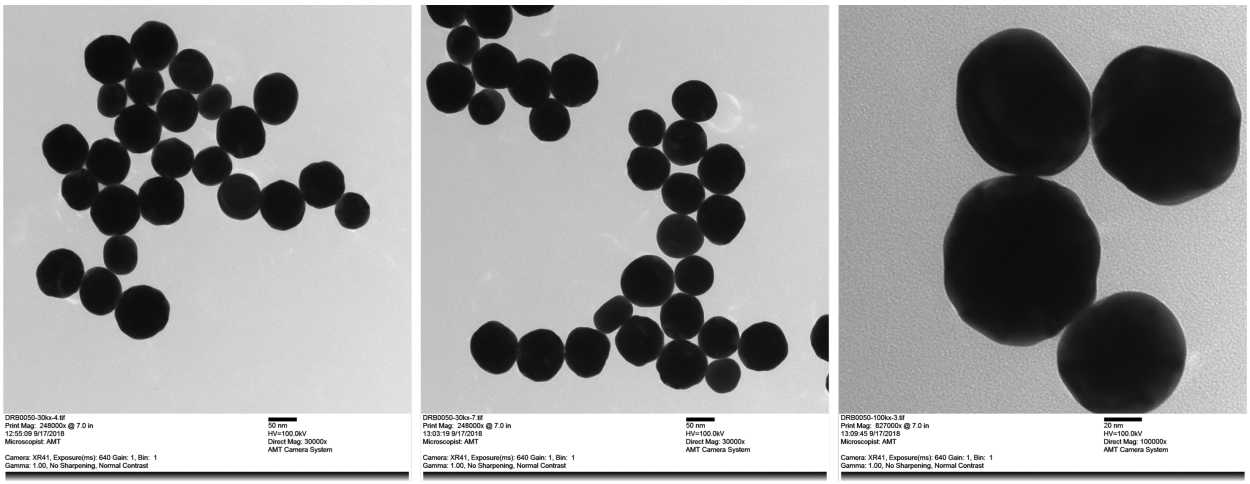

FIG. S9. TEM images of the 80 nm NanoXact AuNPs.